Pigments and microstructure of the colour polymorphic shells of *Polymita picta* and *P. muscarum* (Gastropoda: Cepolidae), with observations on a new light-transmitting shell spot system

Mario Juan Gordillo-Pérez*[1] https://orcid.org/0000-0003-2264-3886; Natalie Beenaerts[1] https://orcid.org/0000-0001-5655-5943 Julia Sigwart[2] https://orcid.org/0000-0002-3005-6246; Thierry Backeljau[3] https://orcid.org/0000-0002-9057-9727; Thomas Vranken[4] https://orcid.org/0000-0001-9724-2054; Javier Vilasó-Cadre[5] https://orcid.org/0000-0001-5172-7136; Martijn Heleven[1] https://orcid.org/0000-0003-3812-4554; Karen Smeets[1] https://orcid.org/0000-0001-9673-8824; Dries Vandamme[4] https://orcid.org/0000-0003-0941-2434; Bernardo Reyes-Tur[6] https://orcid.org/0000-0002-7955-561X

[1] Hasselt University, Centre for Environmental Sciences, Belgium

[2] Senckenberg Research Institute and Museum of Natural History Frankfurt, Germany

[3] Royal Belgian Institute of Natural Sciences, OD Taxonomy and Phylogeny & University of Antwerp, Department of Biology, Belgium

[4] Hasselt University, Institute for Materials Research, Belgium

[5] Universidad Autónoma de San Luis Potosí, México

[6] University of Oriente, Department of Biology and Geography, Cuba

ABSTRACT

Colour polymorphism in the Cuban painted snails *Polymita picta* and *P. muscarum* is striking, yet the pigmentary and structural bases remain unclear. We combined spectrophotometric screening, Raman micro-spectroscopy, scanning electron microscopy (SEM) and LED transillumination to link pigments, ultrastructure and optics across shell morphs. Melanin standard (*Sepia officinalis*) yielded a robust linear calibration used to quantify total melanin pigments at 215 nm in pooled extracts. Melanin was detected in all samples with predominance in darker morphs. Raman spectra (785 nm) confirmed aragonite mineral organization and revealed carotenoid bands, consistent with a mixed-pigment model in which carotenoids contribute to ground and band colours and melanins underlie darker elements. SEM showed a canonical crossed-lamellar wall with alternating transverse and co-marginal tiers. At “spot” domains surfaces were cribose; fracture exposed locally disordered, more porous mineral arrangement enriched in organic matrix, bounded basally by an organic layer. We understand these as a photo-transmissive system in terrestrial gastropods probably overlooked. Under transillumination, spots acted as discrete light-transmitting windows, abundant in *P. muscarum* and sparse in *P. picta*. We propose a pigment-structure-optics framework, in which pigments and microstructural

packing jointly play potential roles in photoprotection and behavioural thermoregulation. These results provide a mechanistic context for colour polymorphism in *Polymita* and suggest testable links to thermal ecology and conservation.

INTRODUCTION

Mollusc shells exhibit an extraordinary diversity of colours, patterns and degrees of transparency resulting from the combined effects of pigment chemistry and shell ultrastructural organization. Together, these factors generate a wide range of optical behaviours, including absorption, scattering and transmission of light. Shell colouration has long attracted attention due to its ecological significance, playing roles in camouflage, signalling, photoprotection, thermoregulation and immune defence; and it is a popular subject studying how phenotypic polymorphisms are evolutionary maintained (Scheil et al., 2013; Mann and Jackson, 2014; Williams, 2017; Davison et al., 2019; Checa et al., 2018; Stuart-Fox et al., 2021; Gefaell et al., 2023). Despite decades of research, however, major knowledge gaps remain regarding the chemical identity of shell pigments, the structural organization of the pigments in the crystalline architecture of the shell and the functional role(s) of shell colour traits in natural populations (Cuthill et al., 2017; Williams, 2017).

Three main classes of pigments are commonly associated with molluscan shell colouration: melanins, carotenoids (polyenes) and porphyrins (Hedegaard et al., 2006; Williams, 2017). Melanins are typically linked to darker patterns and bands, whereas carotenoids contribute to yellow, orange and pink hues, and porphyrins have been associated with a variety of shell colours which may generate fluorescence under ultraviolet excitation (Speiser et al., 2014; Williams, 2017). However, these associations are not universal, and pigment composition can vary considerably even among closely related taxa (Verdes et al., 2015; Affenzeller et al., 2020b).

The genus *Polymita* H. Beck, 1837 (Gastropoda: Cepolidae) comprises six species of tree land snails endemic to Eastern Cuba (Lewis et al., 2025) and is renowned for its striking shell colour polymorphism (Reyes-Tur et al., 2025). Yet, the shell pigments that are responsible for shell colour in *Polymita* were hitherto only investigated by Comfort (1951), who focussed on *Polymita picta* (Born, 1778). That study reported the presence of melanins -not declared method- and a negative murexide test on intact shells, that together with the absence of characteristic ultraviolet fluorescence, suggested that porphyrins derived from heme degradation (e.g. uroporphyrins) were unlikely to be

present. To date, no comprehensive analyses have assessed pigment diversity, relative abundance or spatial distribution within *Polymita* shells, severely limiting our understanding of the molecular and evolutionary bases of their conspicuous colour polymorphism.

Shell colouration can have important functional consequences by influencing thermoregulation, photoprotection and ecological interactions (Stuart-Fox et al., 2021; Gordillo-Pérez et al., 2025). In taxa such as *Polymita* that can inhabit open, sun-exposed environments (González-Guillén, 2021), variation in pigment composition and shell ultrastructure may strongly affect heat absorption, thermal performance and tolerance to thermal stress (Seuront et al., 2018; Schweizer et al., 2019). In addition, highly conspicuous colour patterns may influence predator-prey interactions, suggesting that shell colour polymorphism could be maintained by multiple and potentially interacting selective pressures (Cuthill et al., 2017).

Gastropod shells are composite biominerals composed mainly of crystalline aragonite and/or calcite (both calcium carbonate) embedded within a minor, but functionally important, organic matrix. Externally shells are covered by the periostracum, a chitin and protein-rich layer that templates early shell mineralization. Both shell and periostracum may host pigments. At the microscale, shells frequently exhibit a crossed-lamellar crystalline microstructure organized hierarchically into first-, second- and third-order lamellae, often combined with prismatic or other crystalline mineral organizations (de Paula and Silveira, 2009; Song et al., 2019; Höche et al., 2020). These structural features can directly influence optical performance, as light propagation in calcium carbonate based composites depends not only on pigment absorption, but also on packing density, porosity and refractive-index contrasts at organic-mineral interfaces (McCoy et al., 2024). Modifications in the mineral arrangement appear in mollusc shells, such as asymmetry in the prismatic layer, as well as tubules, tunnels, or pores that extend fully or partially through the shell wall (e.g. Oberling, 1955, 1964; Batten, 1984; Kiel, 2004; Okada et al., 2009; Chen et al., 2021; Páll-Gergely, 2025). These structures have been associated with muscle insertions and/or the exchange of gases, water and ions. In bivalves, specialized aragonitic “windows” channel light in a manner alike to fibre-optic systems (McCoy et al., 2024) and in polyplacophorans (chitons), shell-integrated sensory systems such as eyes or aesthetes exploit mineral structures to transmit light to underlying tissues (Ampuero et al., 2024; Varney et al., 2024); however, whether comparable light-transmitting

mechanisms occur in terrestrial gastropods remains largely unexplored.

Polymita picta and *P. muscarum* (I. Lea, 1834) display exceptional shell colour diversity, including highly variable background colours, banding patterns and irregularly distributed "spots" that generate diffuse black, brown or reddish areas in pigmented shells (de la Torre, 1950) and appear translucent in totally white shells. These spots have been suggested to play a functional role in luminance modulation (Gordillo-Pérez et al., 2025). Although this extreme polymorphism has made *Polymita* a potential model for investigating the evolution and maintenance of colour diversity in terrestrial gastropods -particularly in Neotropical regions where such studies are scarce- despite, mechanisms underlying this variability remain poorly understood (Davison, 2002). The six *Polymita* species in Cuba are threatened by climate change, habitat loss and poaching (CITES, 2025). As shell colouration is one of the most conspicuous traits driving their exploitation, elucidating the pigmentary and structural bases of shell colour is not only essential for evolutionary biology but also highly relevant for conservation. Knowledge of the mechanisms underlying colour variation may help assess the loss of phenotypic diversity, identify potentially vulnerable morphs and evaluate the adaptive significance of colour under climate changing conditions. Therefore, we investigate in this study the pigment composition and shell ultrastructure across colour morphs of *P. picta* and *P. muscarum*, considering their potential ecological significance and implications for conservation.

MATERIAL AND METHODS

Samples and phenotype classification

Due to the threatened status of *Polymita picta* and *P. muscarum* and hence the remarkable value of its biological collections, as little as possible destructive sampling was applied. Whenever possible, visually well-preserved but previously broken shells belonging to the collection of the Terrestrial Molluscs Captivity Breeding Laboratory of Universidad de Oriente, Cuba were used to analyse pigments and shell ultrastructure. We assigned shells and shell fragments to seven colour morphs of *P. picta* [Black (Bl), Red-Orange (R), Green (G), Brown (B), Black Banded Yellow (bbY), Pink Banded Yellow (pbY) and White (W)] and five colour morphs of *P. muscarum* [Black banded brown (bbB), White Banded Brown (wbB), Unbanded Brown (unbB), Black Banded White (bbW) and Unbanded White

(unbW)] following Alfonso and Fernández (1992) and Alfonso and Berovides (1989). No permits were required for the described study, which complied with all relevant regulations.

Melanin detection in shells using UV-visible spectrometry

Shells were pretreated and total melanin was extracted following Hao et al., (2015) and Afenzeller et al., (2020). Shell fragments were cut so as to obtain pieces with either only the background colours or only colour bands. These pieces were washed in deionized water, dried and weighed. Between 53 and 890.6 mg of shell belonging to 1-3 individuals per colour morph were placed in tubes with 3 mL of 6 mol/L HCL for over 12 h to hydrolyse shell proteins (Supplementary Data 5: https://doi.org/10.5281/zenodo.17342893). Next, these tubes were centrifuged at 3000 rpm for 5 min after which the supernatant was discarded. At this point another 3 mL of 6 mol/L HCl was added to the tubes which were subsequently incubated for 1 h in boiling water to finish protein hydrolysis. The remanent undissolved portions were washed three times with deionized water and again centrifuged at 3000 rpm for 5 min. Next, the precipitated pigmented powder in each tube was dried at 80 °C and dissolved in 2 mL of 0.01 mol/L NaOH. For each precipitate, the UV absorptions (range of 190-500 nm) were scanned using a Cary 5000 UV-Vis-NIR Spectrophotometer from Agilent Technologies. The 0.01 mol/L NaOH solution was used as a blank. The presence of melanin was inferred from a broadband, monotonically decreasing absorbance from the UV to the visible range (Hao et al., 2015). Finally, curves were plotted using Cary WinUV software version 5.3.

Melanin quantification in shells

A standard stock solution of commercial *Sepia officinalis* (95%; Sigma-Aldrich, St. Louis, MO, USA) melanin (1 mg/mL) was prepared in 0.01 mol/L NaOH under constant stirring for 2 h at room temperature to completely dissolve the melanin in dark conditions. Working solutions were prepared by serial dilution of the stock to final concentrations of 40, 80, 160, 240, 320, 400 and 480 µg/mL. A solvent blank was measured at the beginning of each analytical run and used for baseline correction. Each concentration standartd was prepared and measured in triplicate.

For each concentration, mean absorbance at 215 nm (Hao et al., 2015) and standard deviation (SD) were calculated across replicates. A calibration curve was fitted by ordinary

least squares linear regression (absorbance vs. concentration) in R (version 4.4.1) (Supplementary Data 6: http://doi.org/10.5281/zenodo.17342922). Model quality was assessed by the coefficient of determination (R^2), analysis of variance of the regression (F statistic), and residual diagnostics (normality and homoscedasticity). Analytical sensitivity parameters were derived from the regression output. The limit of detection (LOD) was calculated as LOD = 3σ/S, and the limit of quantification (LOQ) as LOQ = 3.33 × LOD (≈ 10σ/S), where S is the slope of the calibration line and σ is the SD of the intercept obtained from the OLS fit.

For each shell pigment precipitate showing a melanin-like spectrum, melanin was quantified at 215 nm using the calibration samples prepared with the commercial *Sepia officinalis* melanin. For each melanin positive precipitate the melanin concentration (C) was determined as C (µg/mL) = (A215 – a)/S, where A215 is the blank-corrected absorbance at 215 nm, and a and S are the intercept and the slope of the calibration curve, respectively. Melanin mass (M) in the precipitate was computed as M (µg) = C (µg/mL) × Vf (mL) × DF, with Vf = 2 mL (final volume of dissolved precipitate for all samples) and DF the appropriate dilution factor of the calibration solution (here 1). The amount of melanin relative to the processed shell mass was expressed as percentage (Lehmann et al., 1996). Estimates outside the calculated working range (40-480 µg/mL) were flagged as “extrapolated” and interpreted cautiously. Results below the LOD were reported as “melanin not detected”, while values between the LOD and LOQ as “melanin detected but not reliably quantifiable”. Reported melanin percentages refer to pooled material of up to three different individual shells and do not capture individual-level variability. For the calibration curve construction and quality parameters application we followed the criteria of Greenwell et al. (2014), Ranke et al. (2018), Conti (2022) and Chand et al. (2023). All data processing was carried out in R (version 4.4.1) (Supplementary Data 7: DOI 10.5281/zenodo.17342967).

Raman spectroscopy

The shell ground colour, as well as the colour of the dark, pink and white bands or spots on the surface of *Polymita picta* and *P. muscarum* shells were examined using microscopic analysis combined with Raman spectroscopy (Renishaw inVia Qontor) using a 785 nm 100 mW laser. A 50x Leica long working distance objective was used, in combination with a 1200 lines/mm grating. Shell fragments were subjected to 10 % laser

(~ 10 mW), with an exposure time of 2 s per accumulation, using 10 accumulations per spectrum. All measurements were performed under ambient conditions.

Scanning electron microscopy (SEM) of shell ultrastructure

The preparation of *Polymita* shells for SEM followed Carter and Ambrose (1989) and de Paula and Silveira (2009). Un-polished and un-etched shell fragments were washed by sonication in distilled water, dried and mounted on SEM stubs using double-sided conductive carbon adhesive tape. One replica of each sample (a fragment of the same shell and region) was coated by gold sputtering to contrast with uncoated pieces. Three preparations at the level of spots in *P. muscarum* shells were hand-polished (not embedded) using SiC abrasive papers (FEPA P-grit) under minimal pressure. Wet grinding was performed using distilled water with ~ 30 % ethanol to limit carbonate dissolution and samples were frequently rinsed. The grit sequence was P320, P600, P1200, P2500 and P4000. The polishing direction was periodically rotated over ~ 90 degrees and continued until scratches from the preceding grid were removed. Shell fragment surfaces were inspected under a stereomicroscope to confirm their flatness and the absence of deep scratches. The fragments were observed and photographed using a Phenom ProX scanning electron microscope (SEM) operated at 15 kV under low-vacuum conditions (1 Pa). Energy dispersive spectroscopy (EDS) was used to discriminate atomic compositions between mineral and organic matrix components in the shells. We proceeded to describe the shell microstructures following the terminology by Carter and Ambrose (1989), Chateigner et al. (2000) and de Paula and Silveira (2009).

Because the ultrastructure of the shell spots suggested potential light-guiding effects, shells were trans-illuminated by white light using an RGB LED base light (3-channel RGB SMD LEDs, Tangle Hardware and Plastic Products). For each trial, shells were placed over a diffuser plate, 2 cm from the light source and imaged inside a darkened enclosure to minimize stray light.

RESULTS

Melanin calibration curve, detection and quantification in shell fragments

A standard calibration curve was generated using commercial *Sepia officinalis* melanin.

Absorbance values increased linearly with melanin concentration in the range of 40-480 µg/mL (Fig. 1). Linear regression analyses yielded the equation y = 0.1306 + 0.0027x with a coefficient of determination R^2 = 0.9936. The slope (S = 0.0027 ± 0.0001) and intercept (a = 0.1306 ± 0.0274) indicated high sensitivity and low background signal, respectively. The residuals were randomly distributed and the low residual standard error (0.038) confirmed the robustness of the model. Based on the SD of the slope, the LOD was calculated as 31 µg/mL and the LOQ as 103.3 µg/mL. The analysis of variance of the regression (F = 781.1, p < 0.001) supported the statistical significance of the model. Together, these parameters demonstrate that the calibration curve is reliable and suitable for quantifying melanin in subsequent experimental samples.

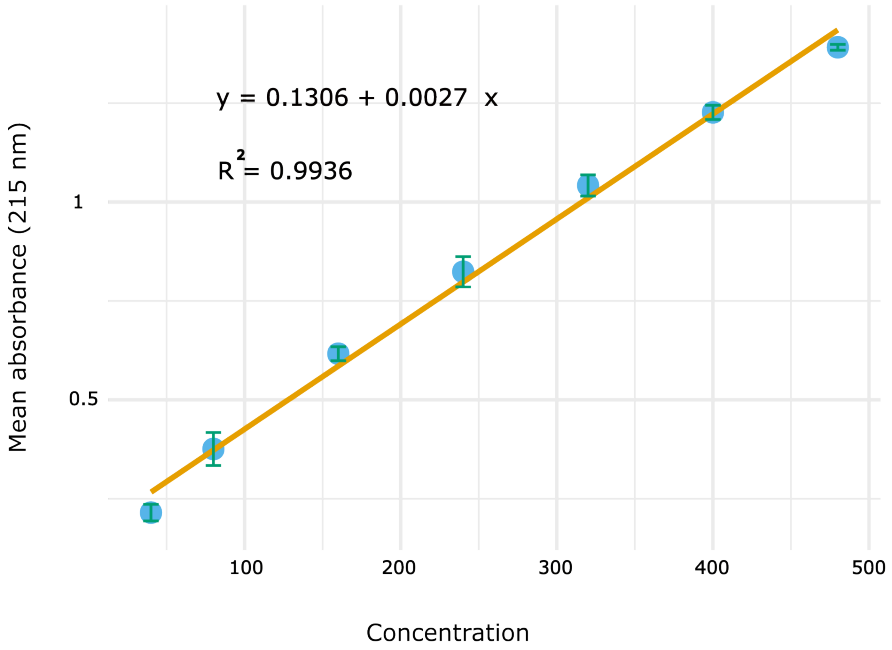

Figure 1. Calibration curve of total melanin concentration in a standard commercial *Sepia officinalis* melanin dilution series of 40, 80, 160, 240, 320, 400 and 480 µg/mL at 215 nm. Means of absorbance and SD are plotted.

Melanin was detected in the 15 precipitates and quantified at 215 nm using the external standard linear *Sepia officinalis* melanin calibration curve (Fig. 2) (Supplementary Data 5: http://doi.org/10.5281/zenodo.17342893). Of these 15 precipitates, nine had melanin concentrations that fell within the validated working range of 40-480 µg/mL and were flagged “in range”, whilesix exceeded this range and were flagged “extrapolated”. These latter should be interpreted as semi-quantitative. Within range, ≥ LOQ concentrations

spanned 128.7-407.5 µg/mL (8 extracts), and one extract was LOD-LOQ (66.5 µg/mL), detected but not reliably quantifiable. Overall, the highest melanin concentrations were observed in *P. picta*: PpBl (0.944 %) (extrapolated), PpR (0.552 %) (extrapolated) and dbPpR (0.337 %). The highest melanin concentration within the validated working range was db-pb PpG inner violet (0.293 %). At the lower end, values included PpB inner violet (0.029 %) (minimum), PmB (0.051%) and Pm albino (0.059 %), with additionally low estimates in *P. muscarum*, PmW (0.102 %) and db PmB (0.145 %). One case (pb PpB inner violet - 0.251%) was detected but not reliably quantifiable (concentration below LOQ) and is therefore reported as LOD-LOQ. These morph-level values are presented as single pooled measurements (no replication) and should be interpreted cautiously; extrapolated estimates denote concentrations outside the validated working range and are semi-quantitative.

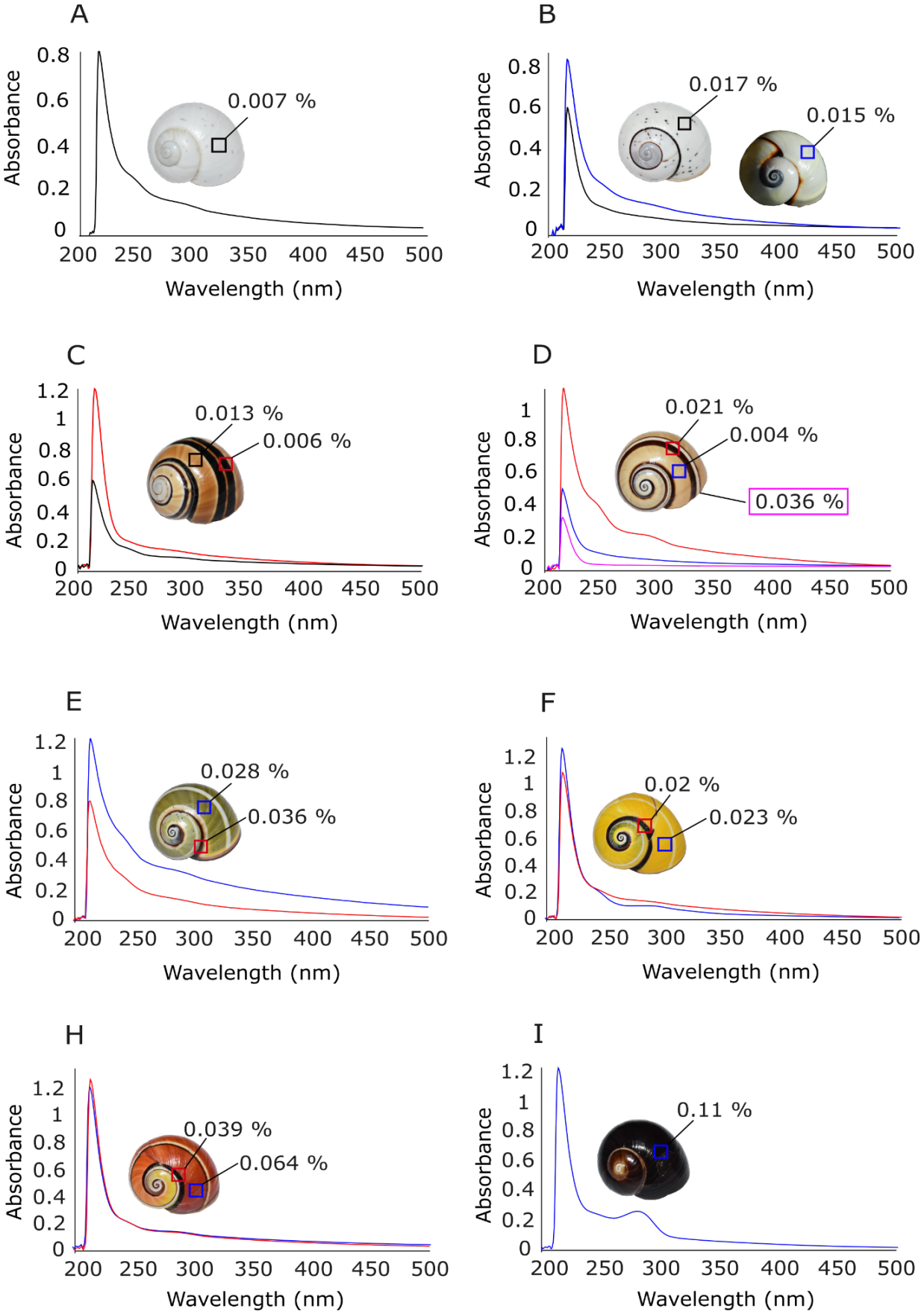

Figure 2. Melanin detection and quantification in pooled fragmented shells of different phenotypes of *Polymita picta* and *P. muscarum*. Percentages of melanin relative to the

pooled shell mass (1-3 individuals per sample) are shown for different shell colours and regions. Panels A-I correspond to the following morphs: A- *P. muscarum* albino; B- *P. muscarum* white; C- *P. picta* white; D- *P. muscarum* dark-banded brown; E- *P. picta* brown; F- *P. picta* green; G- *P. picta* yellow; H- *P. picta* red and I- *P. picta* black. Coloured rectangles indicate the shell region analysed, matching the colour of the corresponding curve. In *P. muscarum*, black represents the background shell colour, while red corresponds to dark bands. In *P. picta*, blue represents the background shell colour, red corresponds to dark bands and pink denotes detection and quantification of melanin in "inner violet-brown" individuals.

Raman spectroscopy

In *Polymita picta*, the Raman spectra acquired with 785 nm laser excitation show a consistent mineral signature across all morphs, characterized by a strong peak at ~1084 cm^{-1} and a well-resolved doublet at 700/704 cm^{-1} (Fig. 3). These peaks correspond to the v_1 and lattice modes of aragonite, indicating a shared calcium carbonate shell structure among all shell colour morphs. In addition, several organic-compound-related bands are detected. In the ground colour of the black morph, bands occur at approximately 1010, 1115, 1292 and 1494 cm^{-1}, the latter appearing as a low-intensity shoulder. The dark band of the red morph exhibits the same set of peaks except for the 1292 cm^{-1} band. In brown shells, these pigment-related peaks are present but with much lower intensity than the aragonite band at 1084 cm^{-1} and the 700/704 cm^{-1} doublet. The ground colour of the red morph displays well-defined bands at 1124 and 1509 cm^{-1}, while the yellow and green morphs show only low-intensity bands at 1136 and 1541 cm^{-1}. Overall, darker morphs show stronger Raman signals in the 1100–1550 cm^{-1} region, consistent with higher organic pigment concentrations, whereas lighter morphs show weaker or nearly flat spectra.

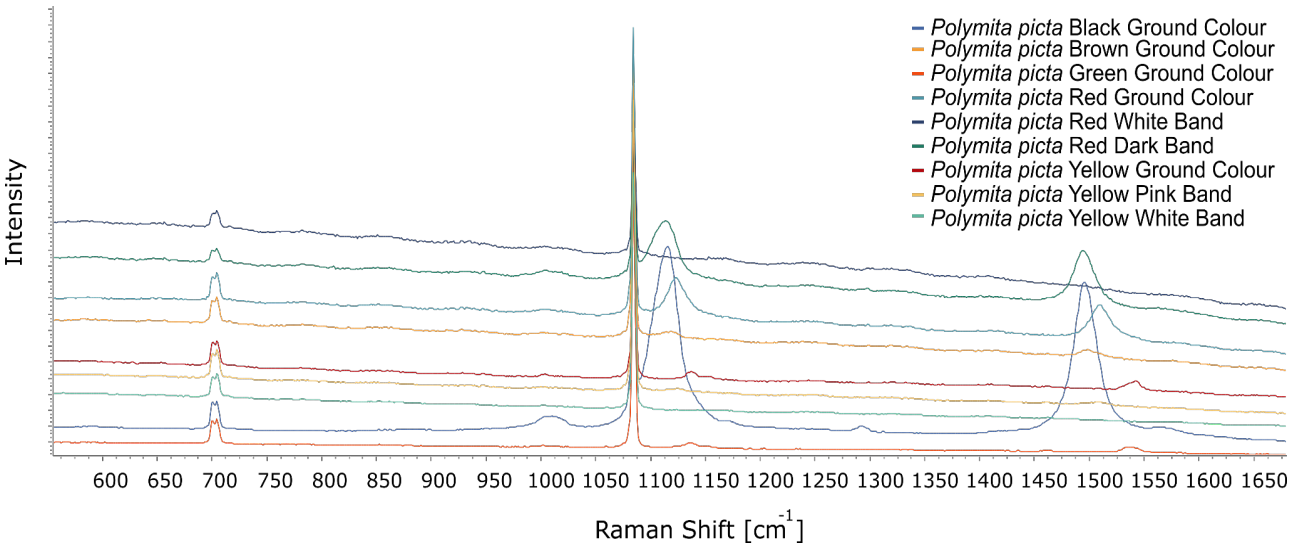

Figure 3. Raman spectra obtained from the ground colour and bands in shell fragments of *Polymita picta*.

Like in *Polymita picta*, all shell colour morphs of *P. muscarum* share the same aragonite signature, with a strong peak at 1084 cm^{-1} and a well-resolved 700/704 cm^{-1} doublet (Fig. 4). Pigment-related bands also appear in darker phenotypes: in the dark band of the brown morph, peaks occur at 1008, 1113, 1293 and 1493 cm^{-1}, the latter presenting a noticeable shoulder. In the ground colour of the brown morph and in the black spots of the white morph, well-defined bands at 1113 and 1493 cm^{-1} are observed. As in *P. picta*, the spectral intensity of these bands is higher in darker regions, indicating higher organic pigment concentrations, while lighter backgrounds show attenuated or minimal pigment signals.

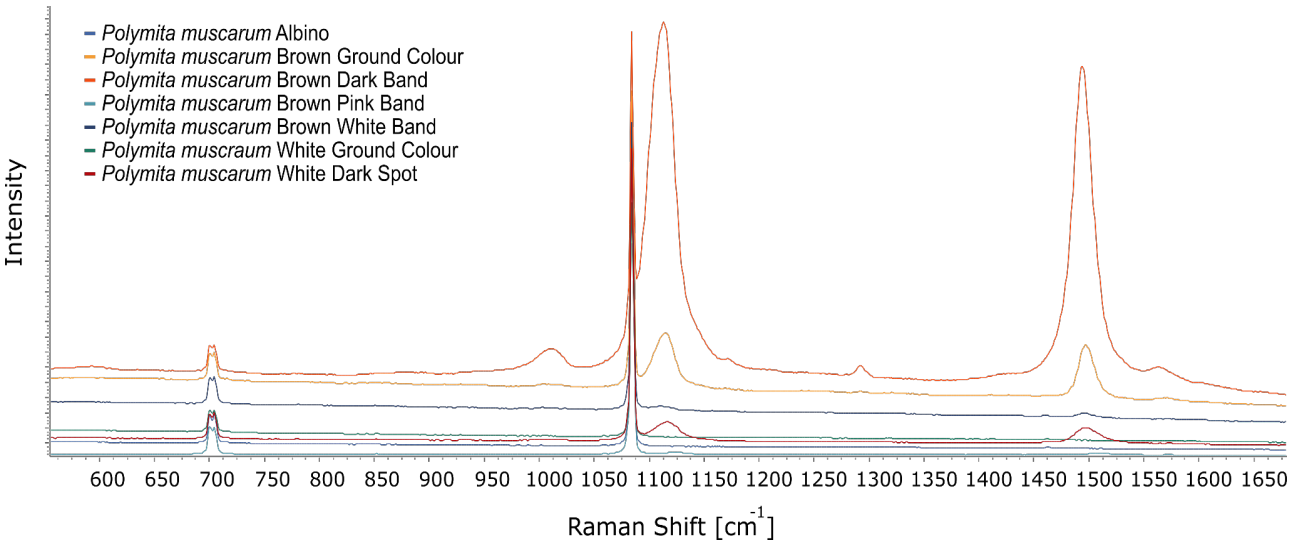

Figure 4. Raman spectra obtained from the ground colour, bands and spots in shell fragments of *Polymita muscarum*.

Scanning electron microscopy (SEM) of shell ultrastructure

The shell wall of *Polymita picta* and *P. muscarum* exhibits a crossed-lamellar architecture with the three canonical hierarchical orders clearly resolved (first, second and third order lamellae) (Fig. 5 A-B). At the finest scale, the lamellae are composed of lath-like irregular prisms; also evidenced in some regions of the periostracum, presenting a typical honeycomb-grid organization (Fig. 5 B and C).

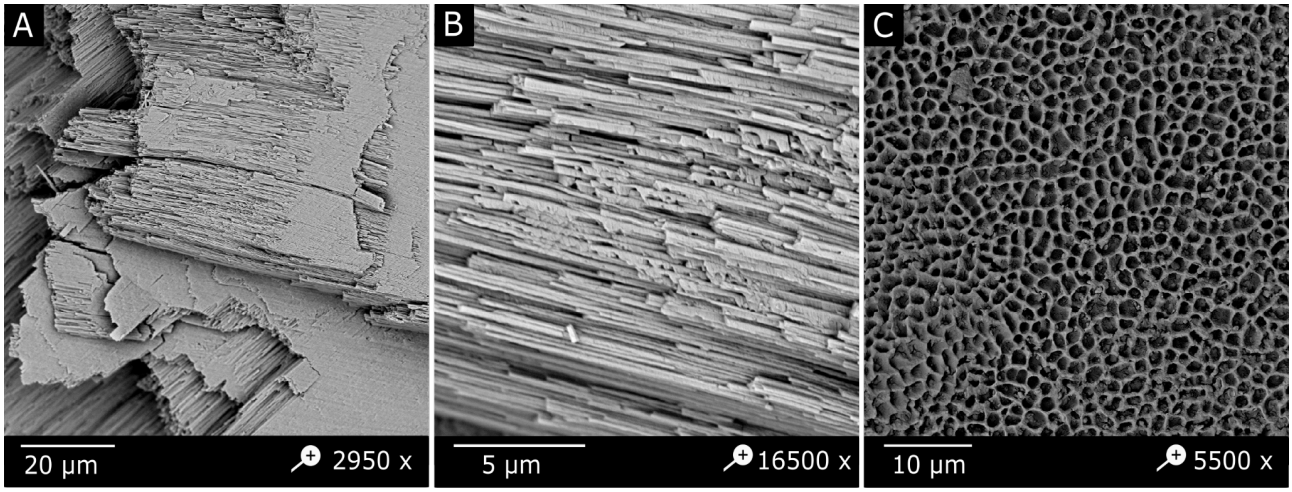

Figure 5. Details of the crossed-lamellar microstructure and the periostracum in the shell o f *Polymita picta* (red morph). A and B: First, second and third order lamellae of the transverse crossed-lamellar layer. C: the honeycomb-grid organization of the shell protein matrix in the outer surface of the periostracum.

First and second order bundles are well delineated and consistently intersect at a characteristic angle of ~ 60°. Local surface relief can occasionally impart a simple prismatic appearance, but the hierarchical arrangement is diagnostic of the crossed-lamellar type. On co-marginal fracture (e.g., fracture parallel to growth lines), the layering from the interior inwards is consistent in both species (Fig. 6).

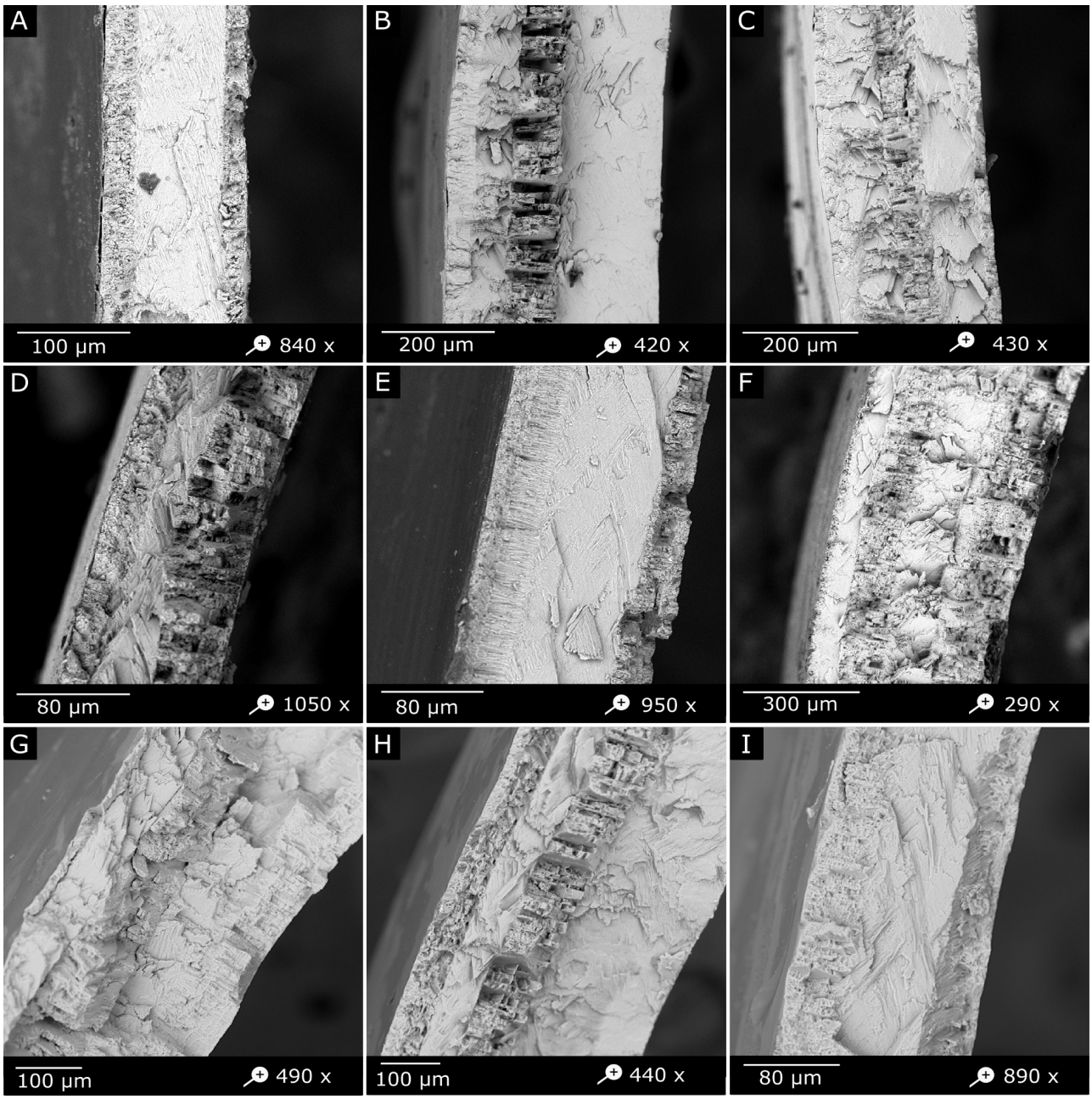

Figure 6. SEM images of co-marginal fractures in shells of *Polymia picta* (Pp) and *Polymita muscarum* (Pm). The periostracum (where presented) and architecture of the layers is presented for the colour morphs A. Pp Black; B. Pp Red; C. Pp Green; D. Pp Brown; E. Pp Yellow; F. Pp White; G. Pm Brown; H. Pm White and I. Pm Albino.

Immediately beneath the periostracum there is an outer crossed-lamellar layer inserted obliquely (~ 45°) relative to the periostracal plane. Within this layer, one set of second order lamellae is oriented approximately normal to the shell surface, while a complementary set of second order lamellae inserts under an angle of ~60° to the first set. Near this outer crossed-lamellar layer, there is a second crossed-lamellar layer, displaying

a similar inter-set angle but with the dominant lamellae arranged transversely to the co-marginal direction. Below this, follows a co-marginal crossed-lamellar layer, which in turn is followed by still another transverse crossed-lamellar layer. Depending on the total shell thickness, these alternating layers (transverse CL-comarginal-transverse CL) repeat inward toward the hypostracum; the number of repetitions and the thickness of individual tiers vary overall shell thickness. Quantitative measures to aid the interpretation of the SEM images are summarized in Supplementary Data 8: http://doi.org/10.5281/zenodo.17343101). These values are provided as reference for figure annotation and are not intended as species level statistics.

Table 1. Measurments of shell layers (mean ± SD) in colour morphs of *Polymita picta* and *P. muscarum*. NA = layer absent or eroded.

Species/ Morph	**Periostacum (µm)**	**Outermost crossed-lamellar layer (µm)**	**Transverse crossed-lamellar (µm)**	**Co-marginal (µm)**	**Transverse crossed-lamellar (µm)**	**Co-marginal (µm)**
***Pp* Black**	1.09 ± 0.22	28.43 ± 1.26	72.86 ± 1.38	23.58 ± 1.89	NA	NA
***Pp* Red**	2.44 ± 0.83	44.60 ± 3.06	63.67 ± 1.21	84.49 ± 1.39	177.95 ± 3.08	
***Pp* Green**	NA	37.11 ± 2.42	71.04 ± 3.31	60.72 ± 1.11	87.50 ± 2.77	16.58 ± 1.36
***Pp* Brown**	1.82 ± 0.57	23.82 ± 2.61	33.00 ± 4.50	54.63 ± 1.04	NA	NA
***Pp* Yellow**	1.87 ± 0.40	44.81 ± 0.70	81.76 ± 1.62	27.99 ± 2.12	NA	NA
***Pp* White**	NA	NA	75.67 ± 2.45	104.04 ± 2.92	135.67 ± 6.80	190.21 ± 5.31
***Pm* Brown**	NA	17.87 ± 3.21	80.16 ± 19.59	79.22 ± 4.14	102.10 ± 6.86	NA
***Pm* White**	NA	61.13 ± 4.85	64.77 ± 2.59	89.74 ± 2.80	210.71 ± 1.82	NA
***Pm* Albino**	NA	49.09 ± 0.90	106.56 ± 1.46	8.90 ± 0.69	NA	NA

At the shell surface there may be spots that form punctate zones, which sometimes are partially covered by the periostracum. Intentional fracturing of shell fragments near such

colour spots exposes their atypical architecture. In general, the spots occur in shell areas where the crystalline structure is less ordered than in the surrounding crossed-lamellar layer, and which show an apparently higher porosity (e.g., larger inter-prismatic spacing) (Figs 7-8). Within spot areas, proteinaceous matrix elements are conspicuous, and the base of the feature is bounded by a distinct organic layer. EDS signals consistent with nitrogen reached up to 22.83 % (Supplementary Data 9: http://doi.org/10.5281/zenodo.17343183), consistent with a potential protein rich phase. In one individual of *P. muscarum* (brown morph), three spot zones showed average "depths" of 17.15 ± 0.27, 10.43 ± 0.16 and 6.60 ± 0.04 µm (Supplementary Data 4: https://doi.org/10.5281/zenodo.17192588).

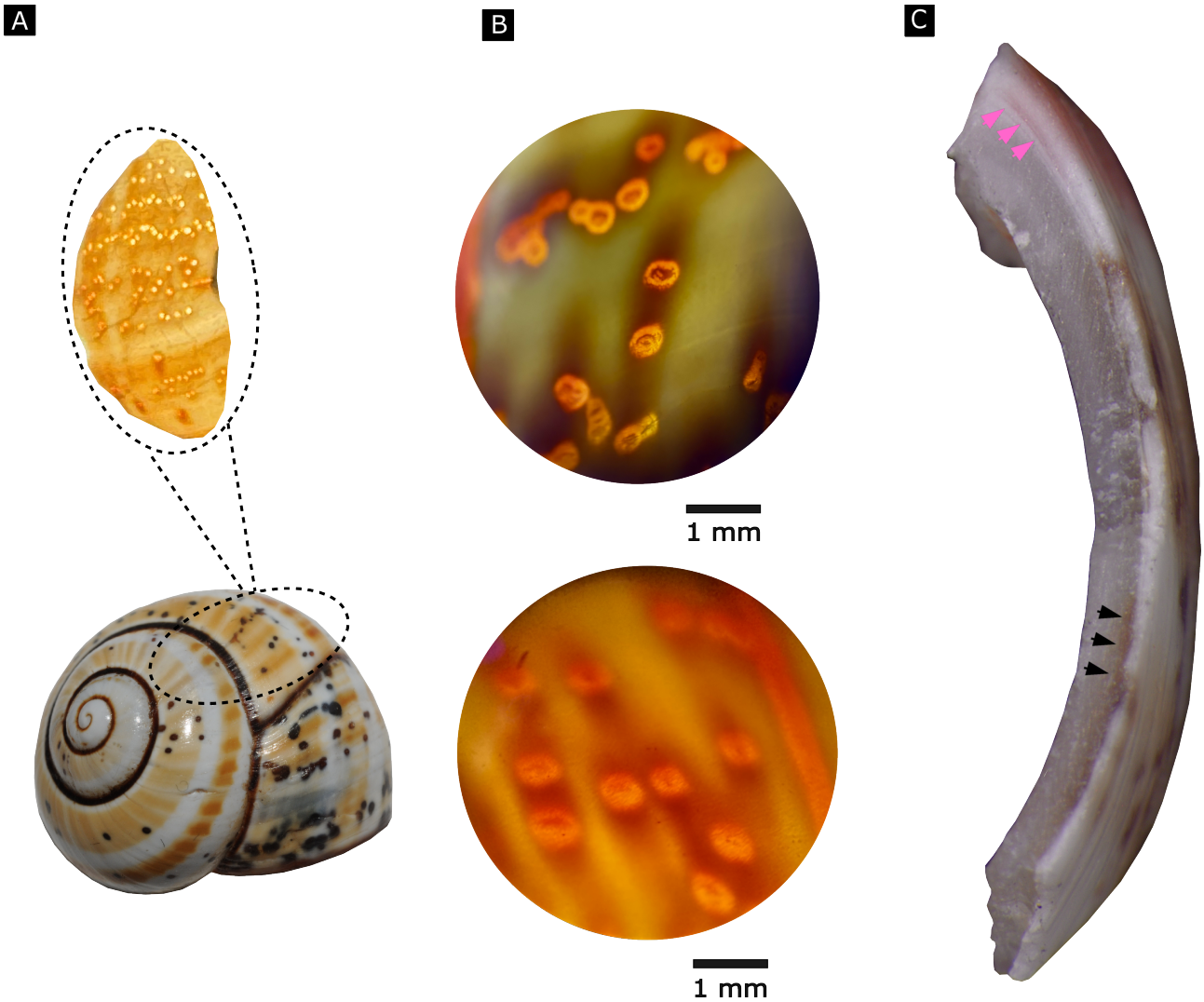

Figure 7. A: Shell fragment with light-transmitting spots in a punctate zone of *Polymita muscarum* (brown morph), transilluminated along the direction of natural light incidence. B:

Light microscopic detail (40x) of the light-transmitting spots in dorsal (upper image) and ventral (bottom image) views. C: Microscopic (56x) transverse view of a *P. muscarum* shell fragment. Black arrows indicate a light-transmitting spot area and an underlying brown band; pink arrows indicate pink pigment deposition layers.

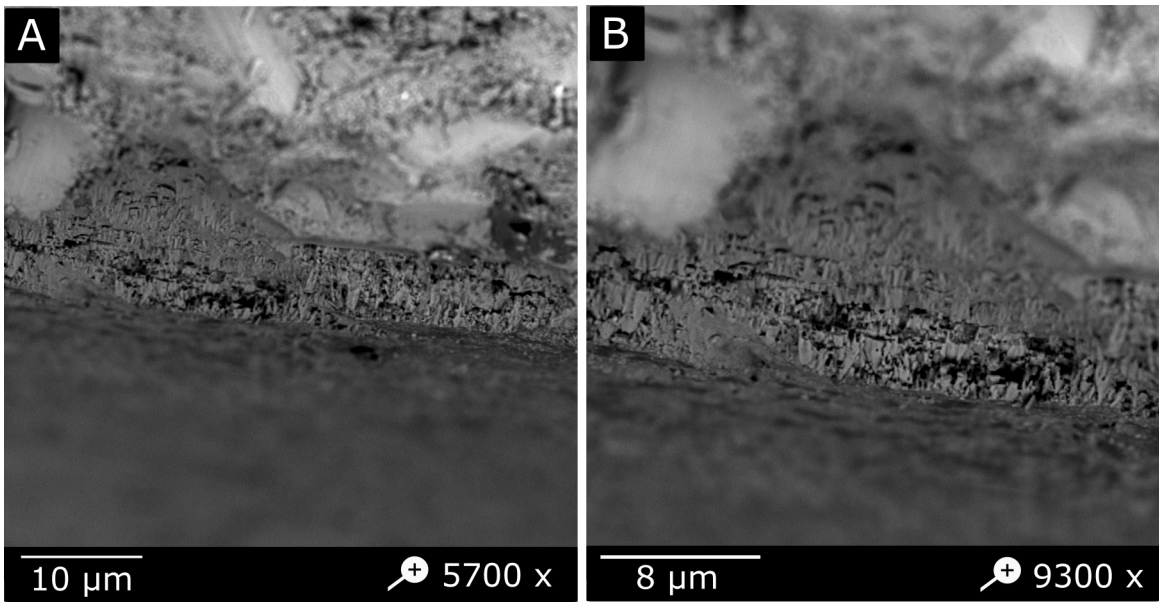

Figure 8. A-B: SEM image of a lateral view of a light-transmitting shell spot in the shell of *Polymita muscarum* (brown morph). In A, contrast with surrounding mineral is observed and the deposit of the organic layer which delimitates the structure. In B, a closer detail of the spot central area covered by periostracum is observed.

Under LED transillumination, shell spots act as a light-transmitting windows, that allow substantially more light to pass than the adjacent shell layers. This effect was consistent across shells, at least for the LED source used herein (Fig. 9). The feature is abundant in *P. muscarum* and only sparsely represented in *P. picta*. In *P. muscarum*, spots occur along most of the spire, extending nearly to the protoconch. Despite their prevalence, no obvious spatial pattern (e.g. periodicity or preferred areas) was discernible at the whole shell scale; the distribution appears irregular within and among whorls.

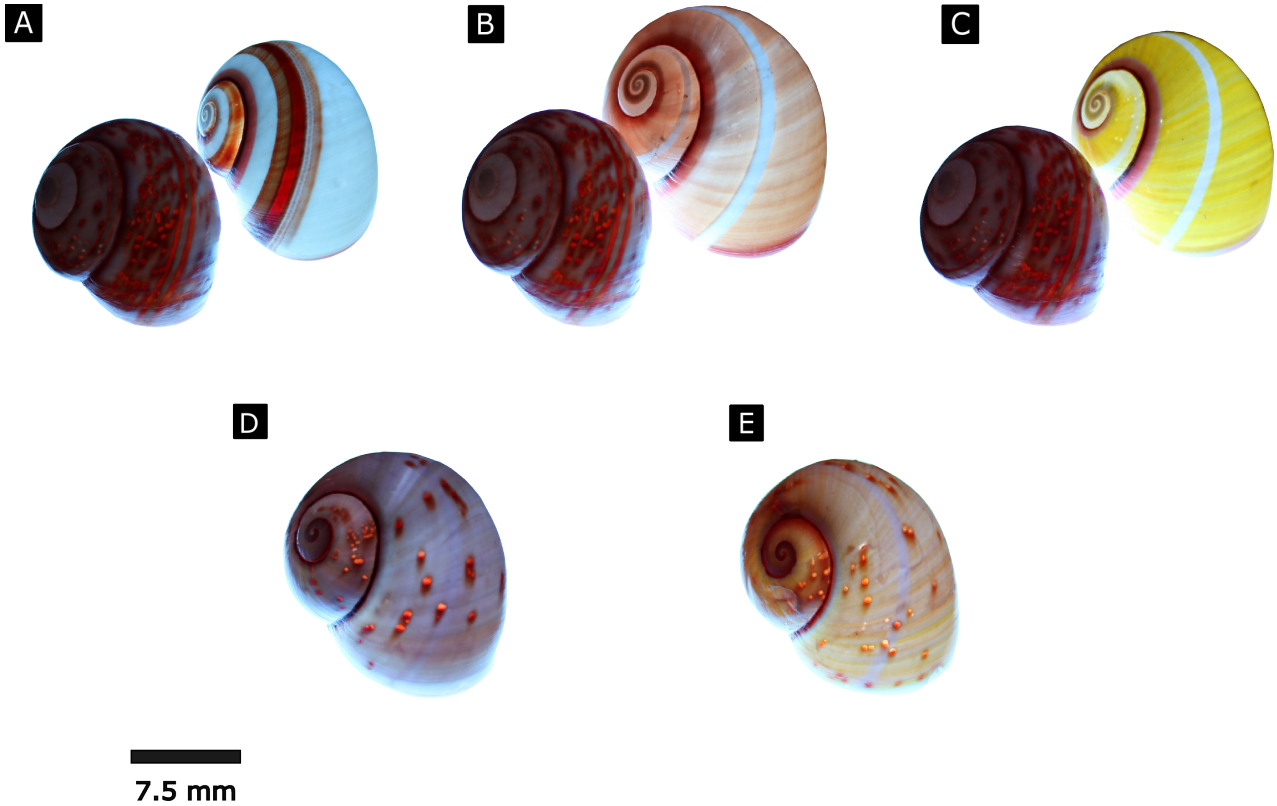

Figure 9. Light-transmitting shell spots in *Polymita* shells revealed by transillumination. A-C: Paired images of a *P. muscarum* (brown-banded white morph; lower left in each pair) compared with *P. picta* morphs (white, brown, and yellow with bands; upper right in each pair). Prominent light-transmitting spot domains are visible in *P. muscarum*, whereas the corresponding *P. picta* shells in A-C lack light-transmitting spots. D-E: Shells of *P. picta* (white and pale yellow morphs, respectively) exhibiting light-transmitting shell colour spot domains similar to those observed in *P. muscarum*.

DISCUSSION

To better understand the possible ecological roles of the colour polymorphism in the shells o f *Polymita picta* and *P. muscarum*, we explored the shell pigments and crystalline ultrastructure of different shell colour morphs of both species.

Presence and concentration of total melanin in shell colour morphs of *Polymita picta* and *P. muscarum*

We identified and quantified total melanin concentrations in the shells of both species by plotting total melanin UV (215 nm) absorbance values obtained from *Polymita* shell fragments on a standard linear calibration curve of *Sepia officinalis* melanin. However, interpreting UV (215 nm) absorbance values must be done cautiously because the peptide backbone exhibits strong far-UV transitions ∏—›∏* ~190 nm; n—›∏* ~220 nm, and other organic compounds also absorb strongly at ~ 200-220 nm (Scopes, 1974; Jiang et al., 2010; Soltani et al., 2019). Nevertheless, this method is actually used with efficiency after a long acid and thermal lysis of the mineral and proteinaceous content of the shells (e.g. Hao et al., 2015). Moreover, the combination of a linear melanin calibration curve and the consistent detection across shell pigment precipitates indicates that melanin is present at quantifiable levels in different shell colour morphs.

Also the quantification of melanin in pooled precipitates as we used should be interpreted carefully because we did not have replicates due to the scarcity of available material.

A second well marked band appeared in the spectrum of the black and brown morphs of *P. picta*. This might be due to the accumulation of pyrrole 2,3-dicarboxylic acid (PDCA), one of the four oxidation products of melanin (Affenzeller et al., 2019a). The thermal properties, which confer a darker colouration at least in *P. picta*, could contribute to the easier occurrence of oxidation reactions and at the same time, these oxidised forms might also become part of the combination which confers colour. These findings align with a growing consensus that melanin contributes to the dark (browns, blacks) colour (Affenzeller et al., 2019b) in molluscan shells, often concentrated in the outer organic-rich layer (periostracum) or colour pattern elements. However, in the colour polymorphic terrestrial snail *Cepaea nemoralis*, it appears that the dark pigment is not eumelanin (Affenzeller et al., 2020).

Raman spectroscopy

The Raman spectroscopy data showed that the shells of both *Polymita picta* and *P. muscarum,* mainly consist of aragonite, consistent with most other pulmonate shells (Alves et al., 2023; Li et al., 2025). Additional bands correspond to the canonical carotenoid resonance Raman triplet, with expected shifts associated with conjugation length, protein interactions and aggregation state (Withnall et al., 2003; Macernis et al., 2014; Udensi et al., 2022; Kolašinac et al., 2025).

Eumelanin typically produces broad D/G-like envelopes around ~1380 and ~1580 cm^{-1}, but

at 785 nm excitation its detection is hampered by strong fluorescence backgrounds and low signal-to-noise ratios (Ferrari et al., 2000; Huang et al., 2004). The absence of clear melanin peaks therefore does not exclude its presence, as supported by independent UV (215 nm) based estimates. A more definitive characterization of eumelanin versus pheomelanin would require alkaline H_2O_2 oxidation followed by HPLC of diagnostic markers, i.e. PTCA and PDCA for eumelanin and TTCA and TDCA for pheomelanin (d'Ischia et al., 2013).

Our findings in carotenoid-related Raman spectra signals are consistent with those reported in neritid shells (Komura et al., 2018), where carotenoids accumulate progressively from inner layers, while black pigmentation is restricted to a narrow surface zone. In *Polymita*, the presence of pronounced polyene bands (Udensi et al., 2002) in (1) the dark colour bands of both species, (2) the black and red ground colours of *P. picta,* and (3) the brown ground colour and spots of *P. muscarum*, supports a mixed-pigment model in which carotenoids and melanins jointly contribute to the observed colour gradients. Notably, spectral variation is more uniform across shell colour morphs in *P. picta*, whereas *P. muscarum* exhibits more chemically distinct pigment signatures among its morphs, indicating that the latter shows stronger differentiation in the composition or relative abundance of organic pigments. This variation likely reflects differences in pigment quantity and specific organic components rather than changes in the underlying mineral matrix.

Together with the previously identified 'indiscrete' luminance patterns -suggesting continuos colour gradients- (Gordillo-Pérez et al., 2025), these findings suggest that colour variation arises from shifts in pigment concentrations and crystalline layering in the shell. Testing these mechanistic hypotheses will require complementary approaches targeting pigment partitioning and vertical distribution within shell layers.

Shell structure and light-transmitting shell colour spots

The SEM photographs showed that both species have a crossed-lamellar shell microstructure comprising first, second and third order lamellae that, intersect at characteristic angles (~ 60° between second order lamellae). In gastropods, this architecture shows a high fracture resistance due to crack deflection at multiple length scales (de Paula and Silveira, 2009; Marin et al., 2012; Rodríguez-Navarro et al., 2012). The alternation of crossed-lamellar layers with co-marginal layers, repeating onward

toward the hypostracum, is consistent with established models of crossed-lamellar layering and with reports of species-specific layer thickness (Checa, 2018). Whether the observed variations between topologically-equivalent layers in *P. picta* are related to intraspecific and/or intra shell colour morph variations should be investigated further.

The periostracum, if present, showed an organic honeycomb-grid consistent with chitin and protein matrices that template mineral deposition and can retain pigments. Histological and biochemical studies emphasize that periostracal and inter crossed-lamellar matrices control nucleation and orientation of aragonite, thereby offering possible sites for pigment deposition or exclusion (Chateigner et al., 2000; de Paula and Silveira, 2009; Nakayama et al., 2013). However, not in every shell fragment of *Polymita*, the periostracum presented the honeycomb-grid organization, for in some cases the outer layer was smooth or partially, if not totally, absent. This demands for further study due to this structure's relevance in colouration and most probably its role in water/humidity retention and exchange.

At the surface of the shell of *Polymita muscarum* and also in some shells of *P. picta* there are shell colour spots in what appear to be matrix-rich porous areas, which differentially interact with light. SEM reveals punctate surfaces which, upon fracture adjacent to spots, show areas with less crystalline order and more porosity (larger inter-prismatic spacing) than the surrounding crossed-lamellar layer. The presence of a conspicuous proteinaceous matrix and a basal organic layer in these areas is consistent with local organic enrichment. Elemental spectrum indicating up to 30.75 % nitrogen within spot domains. However, quantitative EDS of light elements (e.g. C, N, O) in heterogeneous, rough biominerals is semi-quantitative at best-low energy Ka lines are readily absorbed, peaks to background ratios are poor, and results depend strongly on geometry and matrix corrections; hence, values should be treated as compositional evidence rather than absolute stoichiometry (Gazulla et al., 2013; Newbury et al., 2015).

Together these features explain the transillumination behaviour of the shells: areas with light-transmitting shell spots (for the LED wavelengths used), function as “windows” that are abundant in *P. muscarum* but sparse in *P. picta*. This light-transmission system has, to the best of our knowledge, not yet been reported before in molluscs. Despite the presence of shell-integrated photonic or visual systems in marine molluscs e.g. chitons eyes or aesthetes (see Lee et al., 2011; Li and Ortiz, 2013; Li et al., 2015; McCoy et al.,2024; Varney et al., 2024; Ampuero et al., 2024), we are not aware of comparable structures in terrestrial gastropods.

The irregular spatial distribution of the light-transmitting shell spots across the spire and their extension toward the protoconch, suggests that the spot are not formed according to a regular periodic morphogenetic patterning. Instead, we hypothesise that their formation, probably by mantle cells, is at least in part governed by both internal and external influences. Irrespective of their formation, the capacity to transmit light makes that the shell colour spots (or the shell areas where these are located) in *Polymita* may act as light "windows" for animals that are withdrawn in their shell. As such, these "windows" could perhaps trigger or modulate a snail's behaviour and/or physiology in relation to, for example, thermoregulation (just to name a plausible factor). Although our observations and hypotheses are consistent with a sensory interpretation, they remain circumstantial. Demonstrating that the light-transmitting shell colour spots in *Polymita* effectively function as a bona fide light sensory system would require targeted behavioural assays under controlled illumination, mapping of light-sensitivity in pallial tissues and exclusion of alternative structural-optical explanations. Yet, optical imaging studies in land snails at least suggest that translucence depends strongly on both shell pigmentation and microstructure (Savazzi and Sasaki, 2013), which is consistent with our observation that in *Polymita* shells surface areas with many colour spots are particularly light transmissive.

A tentative integrative interpretation of colour polymorphism in *Polymita*

The joint presence of melanin and carotenoids in *Polymita* shells provides the basis for their shell colour polymorphism, as is also seen in other terrestrial gastropods . Both pigment classes (and potentially their oxidation products) may buffer light radiation and heat stress by altering light absorbance and dissipation (Emberton et al., 1963; Schweizer et al., 2019; Gordillo-Pérez et al., 2025). This view hence reflects the hypothesis that shell colour polymorphism in *Polymita* has a thermoregulatory function, based on the spatially heterogeneous distribution of pigments that could help stabilizing body temperature under fluctuating insulation.

In this view, the crossed-lamellar shell architecture is not a passive backdrop, but instead provides a hierarchical interface by its variable inter-lamellar spacing that creates a micro-framework for an organic matrix that regulates crystalline orientation and pigment location, which via local refractive-index contrast and scattering, optical behaviour (Rodríguez-Navarro et al., 2012; Osuna-Mascaró et al., 2014; Bonnard et al., 2020; Agbaje et al., 2021)..

Further and in-depth studies exploring the structural biology in *Polymita* shells on the organisation of pigments and minerals, the ecological interactions of these structural elements, their origin and evolution will reveal relevant topics for conservation management, as well as thermoresistance and climate change adaptation.

REFERENCES

Affenzeller S, Frauendorf H, Licha T, Jackson DJ, Wolkenstein K. Quantitation of eumelanin and pheomelanin markers in diverse biological samples by HPLC-UV-MS following solid-phase extraction. PLoS One. 2019;14(10):e0223552.

Affenzeller S, Wolkenstein K, Frauendorf H, Jackson DJ. Eumelanin and pheomelanin pigmentation in mollusc shells may be less common than expected: insights from mass spectrometry. Frontiers in Zoology. 2019;16(1):47.

Affenzeller S, Wolkenstein K, Frauendorf H, Jackson DJ. Challenging the concept that eumelanin is the polymorphic brown banded pigment in *Cepaea nemoralis*. Scientific Reports. 2020;10(1):2442.

Agbaje OB, Dominguez JG, Jacob DE. Organic biopolymers of venus clams: Collagen-related matrix in the bivalve shells with crossed-lamellar ultrastructure. Biochemistry and Biophysics Reports. 2021;26:100939.

Alfonso M, Berovides V. Fenotipos de los morfos de colour y bandas de la concha en *Polymita picta roseolimbata* (Mollusca: Pulmonata) de Maisí (Cuba). Revista de Biología. 1989;3:213-22.

Alfonso M, Fernández A. Patrones fenotípicos de colouración y bandas de la concha en *Polymita muscarum* (Gastropoda: Fruticicollidae) de Holguín, Cuba. Ciencias Biológicas.

1992;24:106-17.

Alves JF, Edwards HG, Korsakov A, De Oliveira LFC. Revisiting the Raman spectra of carbonate minerals. Minerals. 2023;13(11):1358.

Ampuero A, Vončina K, Parkinson DY, Sigwart JD. Aesthete pattern diversity in chiton clades (Mollusca: Polyplacophora): balancing sensory structures and strength in valve architecture. Journal of Morphology. 2024;285(11):e21784.

Batten RL. Shell structure of the Galapagos Rift limpet *Neomphalus fretterae* McLean 1981, with notes on muscle scars and insertions. American Museum Novitates; no. 2776. 1984.

Bonnard M, Cantel S, Boury B, Parrot I. Chemical evidence of rare porphyrins in purple shells of *Crassostrea gigas* oyster. Scientific Reports. 2020;10(1):12150.

Carter JG, Ambrose WW. Techniques for studying molluscan shell microstructure. The Paleontological Society Special Publications. 1989;4:101-19.

Chand DA, Scadeng M, Dieriks BV. Absolute quantification of neuromelanin in formalin-fixed human brains using absorbance spectrophotometry. PLoS One. 2023;18(7):e0288327.

Chateigner D, Hedegaard C, Wenk H-R. Mollusc shell microstructures and crystallographic textures. Journal of Structural Geology. 2000;22(11-12):1723-35.

Checa AG. Physical and biological determinants of the fabrication of molluscan shell microstructures. Frontiers in Marine Science. 2018;5:353.

Chen C, Han Y, Copley JT, Zhou Y. A new peltospirid snail (Gastropoda: Neomphalida) adds to the unique biodiversity of Longqi vent field, Southwest Indian Ridge. Journal of Natural History. 2021;55(13-14):851-66.

CITES S. Convention on International Trade in Endangered Species of Wild Fauna and Flora: Appendices I, II and III: valid from 7 February 2025. 2025.

Comfort A. The pigmentation of molluscan shells. Biological Reviews. 1951;26(3):285-301.

Conti M. ICH Q2 (R2) & Q14 Guidelines and impact on validation in OMCL Laboratories. 2022.

Cuthill I, Allen W, Arbuckle K, Caspers B, Chaplin G, Hauber M, et al. The biology of colour. Science 357: eaan0221. 2017.

d'Ischia M, Wakamatsu K, Napolitano A, Briganti S, Garcia-Borron JC, Kovacs D, et al. Melanins and melanogenesis: methods, standards, protocols. Pigment Cell & Melanoma Research. 2013;26(5):616-33.

Davison A. Land snails as a model to understand the role of history and selection in the origins of biodiversity. Population Ecology. 2002;44(3):129-136.

Davison A, Jackson HJ, Murphy EW, Reader T. Discrete or indiscrete? Redefining the colour polymorphism of the land snail *Cepaea nemoralis*. Heredity. 2019;123(2):162-75

de la Torre C. El Género *Polymita*. Memorias de la Sociedad Cubana de Historia Natural

¨Felipe Poey¨. 1950;XX, No 1:5-20.

de Paula SM, Silveira M. Studies on molluscan shells: contributions from microscopic and analytical methods. Micron. 2009;40(7):669-90.

Emberton L, Bradbury S. Transmission of light through shells of *Cepaea nemoralis* L. Journal of Molluscan Studies. 1963;35(5):211-9.

Ferrari AC, Robertson J. Interpretation of Raman spectra of disordered and amorphous carbon. Physical review B. 2000;61(20):14095.

Gazulla M, Rodrigo M, Blasco E, Orduña M. Nitrogen determination by SEM-EDS and elemental analysis. X-Ray Spectrometry. 2013;42(5):394-401.

Gefaell J, Galindo J, Rolán-Alvarez E. Shell colour polymorphism in marine gastropods. Evolutionary Applications. 2023;16(2):202-22.

González-Guillén A. *Polymita* uncoiled. 1st ed. Collierville: Memphis: Fundcraft Publishing; 2021.

Gordillo-Pérez MJ, Beenaerts N, Sánchez DL, Smeets K, Arias-Sosa YC, Reyes-Tur B. Shell colour luminance of Cuban painted snails, *Polymita picta* and *Polymita muscarum* (Gastropoda: Cepolidae). PLoS One. 2025;20(1):e0314008.

Greenwell BM. Topics in statistical calibration: Air Force Institute of Technology; 2014.

Greenwell BM, Schubert Kabban CM. investr: an R package for inverse estimation. 2014.

Hao S, Hou X, Wei L, Li J, Li Z, Wang X. Extraction and identification of the pigment in the adductor muscle scar of Pacific oyster *Crassostrea gigas*. PLoS One. 2015;10(11):e0142439.

Hedegaard C, Bardeau J-F, Chateigner D. Molluscan shell pigments: an in situ resonance Raman study. Journal of Molluscan Studies. 2006;72(2):157-62.

Höche N, Peharda M, Walliser EO, Schöne BR. Morphological variations of crossed-lamellar ultrastructures of *Glycymeris bimaculata* (Bivalvia) serve as a marine temperature proxy. Estuarine, Coastal and Shelf Science. 2020;237:106658.

Huang Z, Lui H, Chen X-K, Alajlan A, McLean DI, Zeng H. Raman spectroscopy of in vivo cutaneous melanin. Journal of Biomedical Optics. 2004;9(6):1198-205.

Jiang J, Abramavicius D, Bulheller BM, Hirst JD, Mukamel S. Ultraviolet spectroscopy of protein backbone transitions in aqueous solution: Combined QM and MM simulations. The Journal of Physical Chemistry B. 2010;114(24):8270-7.

Kiel S. Shell structures of selected gastropods from hydrothermal vents and seeps. Malacologia. 2004;46(1):169-84.

Kolašinac SM, Pećinar I, Gajić R, Mutavdžić D, Dajić Stevanović ZP. Raman spectroscopy in the characterization of food carotenoids: Challenges and prospects. Foods. 2025;14(6):953.

Komura T, Kagi H, Ishikawa M, Yasui M, Sasaki T. Spectroscopic investigation of shell pigments from the family Neritidae (Mollusca: Gastropoda). In: Name (Editor),

Biomineralization: From Molecular and Nano-structural Analyses to Environmental Science: Springer Singapore, Singapore; 2018. p. 73-82.

Lee S-W, Jang Y-N, Kim J-C. Characteristics of the aragonitic layer in adult oyster shells, *Crassostrea gigas*: structural study of myostracum including the adductor muscle scar. Evidence-Based Complementary and Alternative Medicine. 2011;2011(1):742963.

Lehmann H, Fuentes-Arderiu X, Bertello L. Glossary of terms in quantities and units in Clinical Chemistry (IUPAC-IFCC Recommendations 1996). Pure and applied chemistry. 1996;68(4):957-1000.

Lewis AM, Reyes-Tur B, Davison A. The mitochondrial genome and phylogenetic placement of the world's most beautiful snail, *Polymita picta*. Journal of Molluscan Studies. 2025;91(2):eyaf006.

Li L, Kolle S, Weaver JC, Ortiz C, Aizenberg J, Kolle M. A highly conspicuous mineralized composite photonic architecture in the translucent shell of the blue-rayed limpet. Nature Communications. 2015;6(1):6322.

Li L, Ortiz C. Biological design for simultaneous optical transparency and mechanical robustness in the shell of *Placuna placenta*. Advanced Materials. 2013;25(16):2344-50.

Li X, Yu X-Y, Zhang C. Mineral Compositions and Organic colour-Related Compounds of Freshwater Bead-Cultured Pearls from Zhuji, Southeast China: Insights from Multi-Spectroscopic Analyses. Crystals. 2025;15(9):824.

Macernis M, Sulskus J, Malickaja S, Robert B, Valkunas L. Resonance Raman spectra

and electronic transitions in carotenoids: a density functional theory study. The Journal of Physical Chemistry A. 2014;118(10):1817-25.

Mann K, Jackson DJ. Characterization of the pigmented shell-forming proteome of the common grove snail *Cepaea nemoralis*. BMC Genomics. 2014;15(1):249.

Marin F, Le Roy N, Marie B. The formation and mineralization of mollusk shell. Frontiers in Bioscience . 2012;4(3):1099-125.

McCoy DE, Burns DH, Klopfer E, Herndon LK, Ogunlade B, Dionne JA, Johnsen S. Heart cockle shells transmit sunlight to photosymbiotic algae using bundled fiber optic cables and condensing lenses. Nature Communications. 2024;15(1):9445.

Nakayama S, Suzuki M, Endo H, Iimura K, Kinoshita S, Watabe S, et al. Identification and characterization of a matrix protein (PPP-10) in the periostracum of the pearl oyster, *Pinctada fucata*. FEBS Open Bio. 2013;3:421-7.

Newbury DE, Ritchie NW. Performing elemental microanalysis with high accuracy and high precision by scanning electron microscopy/silicon drift detector energy-dispersive X-ray spectrometry (SEM/SDD-EDS). Journal of Materials Science. 2015;50(2):493-518.

Oberling J-J. Observations on some structural features of the pelecypod shell. Mitteilungen der Naturforschenden Gesellschaft in Bern. 1964;20:1-60.

Oberling JJ. Shell structure of west American Pelecypoda. Journal of the Washington Academy of Sciences. 1955;45(4):128-30.

Okada S, Chen C, Watsuji T-o, Nishizawa M, Suzuki Y, Sano Y, et al. The making of natural iron sulfide nanoparticles in a hot vent snail. Proceedings of the National Academy of Sciences of the USA. 2019;116(41):20376-81.

Osuna-Mascaró A, Cruz-Bustos T, Benhamada S, Guichard N, Marie B, Plasseraud L, et al. The shell organic matrix of the crossed lamellar queen conch shell (*Strombus gigas*). Comparative Biochemistry and Physiology Part B: Biochemistry and Molecular Biology. 2014;168:76-85.

Páll-Gergely B. *Boucardicus* must have microtunnels! Reassignment of three species into *Acroptychia* (Gastropoda: Caenogastropoda: Hainesiidae). Zootaxa. 2025;5666(2):287-93.

Ranke J. chemCal: Calibration functions for analytical chemistry. R package version 02. 2018;1.

Ranke J, Wöltjen J, Meinecke S. Comparison of software tools for kinetic evaluation of chemical degradation data. Environmental Sciences Europe. 2018;30(1):17.

Reyes-Tur B, Chen Z, Gordillo-Pérez MJ, Ben Hamadou A, Gerheim C, Greve C, Sigwart JD. Draft genome of the Cuban Painted Landsnail *Polymita picta*, International Mollusc of the year 2022. BMC Genomic Data. 2025;26(1):63.

Rodriguez-Navarro AB, Checa A, Willinger M-G, Bolmaro R, Bonarski J. Crystallographic relationships in the crossed lamellar microstructure of the shell of the gastropod *Conus marmoreus*. Acta Biomaterialia. 2012;8(2):830-5.

Savazzi E, Sasaki T. Observations on land-snail shells in near-ultraviolet, visible and near-infrared radiation. Journal of Molluscan Studies. 2013;79(2):95-111.

Scheil AE, Hilsmann S, Triebskorn R, Köhler HR. Shell colour polymorphism, injuries and immune defense in three helicid snail species, *Cepaea hortensis*, *Theba pisana* and *Cornu aspersum maximum*. Results in Immunology. 2013;3:73–78.

Schweizer M, Triebskorn R, Köhler HR. Snails in the sun: Strategies of terrestrial gastropods to cope with hot and dry conditions. Ecology and Evolution. 2019;9(22):12940-60.

Scopes RK. Measurement of protein by spectrophotometry at 205 nm. Analytical Biochemistry. 1974;59(1):277-82.

Seuront L, Terence PTNg, Lathlean JA. A review of the thermal biology and ecology of molluscs, and of the use of infrared thermography in molluscan research. Journal of Molluscan Studies. 2018;84(3):203-32.

Soltani S, Ojaghi A, Robles FE. Deep UV dispersion and absorption spectroscopy of biomolecules. Biomedical Optics Express. 2019;10(2):487-99.

Song X, Liu Z, Wang L, Song L. Recent advances of shell matrix proteins and cellular orchestration in marine molluscan shell biomineralization. Frontiers in Marine Science. 2019;6:41.

Speiser DI, DeMartini DG, Oakley TH. The shell-eyes of the chiton *Acanthopleura granulata* (Mollusca, Polyplacophora) use pheomelanin as a screening pigment. Journal of Natural History. 2014;48(45-48):2899-911.

Stuart-Fox D, Aulsebrook A, Rankin KJ, Dong CM, McLean CA. Convergence and divergence in lizard colour polymorphisms. Biological Reviews. 2021;96(1):289-309.

Udensi J, Loughman J, Loskutova E, Byrne HJ. Raman spectroscopy of carotenoid compounds for clinical applications—a review. Molecules. 2022;27(24):9017.

Use IICfHoTRfPfH. ICH Harmonized Guidelines. Validation of analytical procedures Q2 (R2). ICH Geneva, Switzerland: European Medicines Agency; 2022.

Varney RM, Speiser DI, Cannon JT, Aguilar MA, Eernisse DJ, Oakley TH. A morphological basis for path-dependent evolution of visual systems. Science 2024;383(6686):983-7.

Verdes A, Cho W, Hossain M, Brennan PL, Hanley D, Grim T, et al. Nature's palette: characterization of shared pigments in colourful avian and mollusk shells. PLoS One. 2015;10(12):e0143545.

Williams ST. Molluscan shell colour. Biological Reviews. 2017;92(2):1039-58.

Withnall R, Chowdhry BZ, Silver J, Edwards HG, de Oliveira LF. Raman spectra of carotenoids in natural products. Spectrochimica Acta Part A: Molecular and Biomolecular Spectroscopy. 2003;59(10):2207-12.